What is the origin of the ferroelectricity in the commensurate low temperature phase of YMn_2O_5?

Tina Weigel,[1] Carsten Richter,[2] Melanie Nentwich,[3] Erik Mehner,[1] Valentin Garbe,[4] Laurence Bouchenoire,[5] Dmitri Novikov,[3] Dirk C. Meyer,[1] and Matthias Zschornak[1]

[1]*Institute of Experimental Physics, Technical University Bergakademie Freiberg, 09596 Freiberg, Germany*

[2]*Leibniz-Institut für Kristallzüchtung, 12489 Berlin, Germany*

[3]*DESY Photon Science, Deutsches Elektronensynchrotron, 22607 Hamburg, Germany*

[4]*Institute of Applied Physics, Technical University Bergakademie Freiberg, 09596 Freiberg, Germany*

[5]*European Synchrotron Radiation Facility, 38000 Grenoble, France*

(Dated: April 19, 2023)

Abstract

The material system YMn_2O_5 has several low temperatures phases, where magnetism and ferroelectricity occur. Especially, the origin of ferroelectricity in the commensurate phase is an open question. Literature agrees upon a magnetically driven principal mechanism from changes in the Mn spin configuration, which may be based either on magnetostriction due to symmetric exchange, the antisymmetric inverse Dzyaloshinskii-Moriya interaction or a combination of the two. These mechanisms are accompanied by specific atomic displacements of ions in the structure. The space group $Pbam$ (55) of the paraelectric phase does not allow the respective polar displacements and a refinement of the charge structure in a lower symmetric phase has not been successful so far, mostly because conventional structure analysis lacks the sensitivity required to resolve the expected positional displacements. We applied the new *Resonantly Suppressed Diffraction* (RSD) method, which is sensitive to minuscule structural changes in the sub-pm-range, in order to resolve potential ionic displacements within a polar space group and shed new light on this controversial discussion.

We measured the energy dependent RSD spectra of carefully selected reflections above and below the phase transition temperature $T_{CM} = 39\,K$. With the data above T_{CM}, we refined the static and dynamic displacements of the paraelectric phase to receive an improved initial model for the structural characterization of the ferroelectric phase. Subsequently, we refined 50 static displacement parameters in the lower symmetric space group $Pb2_1m$, which allows polarization in b-direction and present the first structure refinement of the commensurate phase in YMn_2O_5. We found a significant displacement of Mn ions and the O partial structure, which results in a calculated absolute spontaneous polarization $P_s = (1.3 \pm 0.4)\,mC\,m^{-2}$, in good agreement with a measured value $P_s = (0.88 \pm 0.06)\,mC\,m^{-2}$. With the presented investigation, we finally confirm that P_s has an ionic contribution and is predominately induced by magnetostriction.

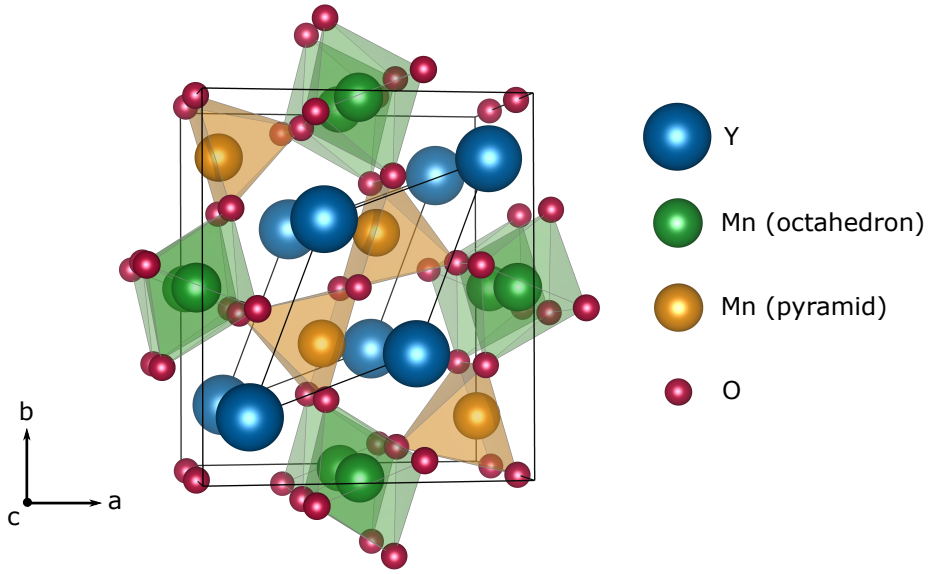

Figure 1. Room temperature P phase of YMn_2O_5 in space group *Pbam* (55).

I. INTRODUCTION

YMn_2O_5 is non-polar at room temperature and crystallizes within the crystallographic space group *Pbam* (55) (see Fig. 1). Mn occupies two different Wyckoff positions in the unit cell, one with octahedral and one with pyramidal oxygen coordination [1].

The material undergoes four phase transitions by lowering the temperature [2–4], see Fig. 2. At $T_{N_1} = 45\,\mathrm{K}$, the structure becomes weakly ferroelectric and antiferromagnetic with a 2-dimensional incommensurate modulation (2D-ICM). Subsequently, a ferroelectric and 1-dimensional incommensurably modulated magnetic phase (1D-ICM) appears between $T_D = 40\,\mathrm{K}$ and $T_{\mathrm{CM}} = T_{C_1} = 39\,\mathrm{K}$. However, most articles only report either T_D or T_{CM} [4–8]. Down to $T_{N_2} = T_{C_2} = 19\,\mathrm{K}$ the structure is commensurately modulated magnetic (CM) in c with an electric polarization in b direction. Below the 19 K transition temperature, the spontaneous polarization changes sign, the structure is weakly

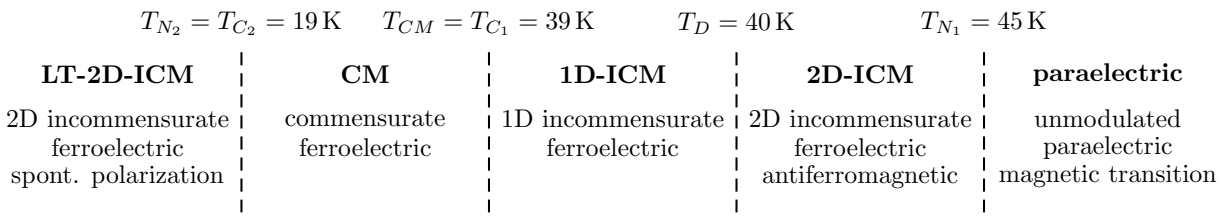

Figure 2. Overview of the four low temperature phase transitions of YMn_2O_5.

ferroelectric and the magnetic moments arrange 2-dimensionally incommensurate, again.

We are interested in the structural changes of the CM phase, which forms between 19 K and 39 K and has an electric polarization in b direction [9, 10]. The CM phase is usually described contradictorily as ferroelectric within the crystallographic space group *Pbam* (55), which is nonpolar and therefore prohibits ferroelectricity (Fig. 1). Apparently, the atomistic origin of ferroelectricity in the CM phase is still not clear. Previous work favors two magnetically induced mechanisms based on changes in the Mn spin configuration - one caused by magnetostriction due to symmetric exchange [9, 11, 12], and the other one caused by the antisymmetric inverse Dzyaloshinskii-Moriya interaction [3, 13], or a combination of both [3, 14–16]. The mechanisms infer certain ionic displacements within the crystal structure. Some of the preceding articles on YMn_2O_5 reported hints about structural changes between the room temperature and the CM phase [4, 6, 17–21]. However, most work did not interpret these data because the magnetic structure was in focus of the research [2, 4–6, 9, 12, 13, 15, 22–34]. Others were explicitly searching for changes but attempts to solve the structures of the CM phase have been inconclusive [35, 36]. Therefore, it is still not clear to what extend the ferroelectric transition can be evidenced in the crystal structure [20, 21, 37]. A possible polar structure in the CM phase is obtained by symmetry descent to space group $Pb2_1m$, which allows a polarization in b direction and which was theoretically proposed [10, 17, 38], but not yet been experimentally observed in YMn_2O_5, because ionic displacements are much smaller than in typical displacive-type

ferroelectrics [35].

In this work, we use a recently developed *Resonant X-ray Diffraction* (RXD) technique to enhance the sensitivity to atomic displacements, to shedding new light on this controversial question discussion about the origin of ferroelectricity in YMn_2O_5. RXD combines diffraction and core-hole spectroscopy and makes use of different physical aspects of the electronic resonance, such as enhanced elemental contrast [39, 40], destructive interference to determine tiny atomic displacements [41] and polarization anisotropy to study short-range order [42, 43], magnetic properties [44, 45], defect structures [42, 46] or electronic properties [47, 48]. Here, we make use of destructive interference in RXD, referred to as *Resonantly Suppressed Diffraction* (RSD), which were demonstrate for the first time in the structural refinement of an electric-field induced polar surface layer in $SrTiO_3$ [41, 49]. Here RSD is used to illuminate ionic contributions to the polarization as a response to the formation of the CM phase.

The identification of ionic contributions to the spontaneous polarization comprises in particular the relevant polar displacements in b direction. To ensure a precise knowledge of the initial structure in terms of static positions as well as dynamic atomic displacements, given by the Atomic Displacement Parameters (ADPs), the paraelectric P phase has been reassessed by means of RSD, prior to the refinement of the CM phase. The results of the structure solutions of P and CM phase are discussed in regard to the goodness-of-fit and a structural origin of the ferroelectricity is provided in conclusion.

II. METHODOLGY

RSD is based on the work of Richter *et al.* [41] and use resonantly tuned extinction evoked by the counterbalance of scattering contributions from different elements in the crystal structure. This effect is expressed by a vanishing structure factor and strongly depends on the crystal structure, the reflection and the X-ray energy. Under such specific

conditions, the intensity of a Bragg reflection approaches zero. The minimum position of the energy-depend intensity is very sensitive to any structural change and provides superior contrast to study atomic displacements on the picometer scale [41].

Following the main idea of the RSD concept, the selection of Bragg reflections is such that the diffraction intensity is minimized while scanning the X-ray energy through the absorption edge and the signal-to-noise ratio is maximized. Reflections are chosen according to a optimized strategy to minimize the required beam time. Based on a starting guess of the structure, calculations of all Bragg reflections yields sensitive candidates for the measurement. Possible sensitive reflections are reassessed in terms of contrast, location of the minimum, and parameter sensitivity. The selected reflections are evualed consequently during the experiment ~~again~~, with each set of measured reflections or newly defined structural degree of freedom. This selection and evaluation of sensitive reflections is not straight forward. In an iterative procedure (more details in Supplemental Material SM Sec. S II), we analyzed the steadily acquired experimental data to obtain an updated list of reflections that are sensitive to prevailing parameter ambiguities.

The structure refinement is based on fitting simulated RSD spectra to the experimental ones to minimize differences, varying the structural degrees of freedom as well as specific experimental parameters. The relative deviation between measurement and calculation was minimized using python's lmfit module [50] for the residuals R, which we defined as the difference between simulated and experimental logarithmic intensities, which is equivalent to the assumption of a constant relative error. The simulated intensities are calculated using the kinematic approximation [51] as

$$I_{\mathrm{kin}} \propto A(E) \cdot |F(E, \boldsymbol{Q})|^2, \tag{1}$$

with the absorption factor $A(E) \approx 1/\mu(E)$ for thick crystals, the photon energy E, the

momentum transfer vector $\boldsymbol{Q}$ and the structure factor $F(E, \boldsymbol{Q})$. The latter is defined as

$$F(E, \boldsymbol{Q}) = \sum_{i=1}^{N} o_i \cdot f_i(E, \boldsymbol{Q}) \cdot \exp(-M_i) \cdot \exp(\mathrm{i}\boldsymbol{Q} \cdot \boldsymbol{r}_i), \tag{2}$$

with the N atoms i, their occupancy of the crystallographic sites o_i, their atomic scattering factors $f_i(E, \boldsymbol{Q})$, their positions in real space $\boldsymbol{r}_i$ and their Debye-Waller-Factors $\exp(-M_i)$, which are related to the atomic displacements $\boldsymbol{u}_i$ in direction of $\boldsymbol{Q}$ according to $M_i = {}^1\!/_2\langle(\boldsymbol{Q} \cdot \boldsymbol{u}_i)^2\rangle$, *i.e.* the mean square projections of the atomic displacements $\boldsymbol{u}_i$ on $\boldsymbol{Q}$ [52] (more details, see SM Sec. S III). The quality of the fit is evaluated by the reduced χ^2 value defined as

$$\chi^2_\nu = \left(\sum_{i=1}^{N} R_i^2\right) / (N - M), \tag{3}$$

with the number of data points N, the number of variables in the fit M.

The general procedure of the analysis is as shown in Fig. 3. In this work, the measured RSD spectra above and below T_{CM} have been fitted in two steps. First the high-temperature P phase has been refined in terms of ADPs and static atomic displacements on the basis of the data above T_{CM}, then changes in the static displacements have been re-evaluated on the bases of the data below T_{CM}.

III. EXPERIMENTAL DETAILS

A. Sample preparation

The YMn_2O_5 crystal (growth described in [53]) has a cuboid shape with an approximate size of 1 mm × 1 mm × 2 mm. We oriented the crystal with a laboratory single crystal X-ray diffraction machine D8 Quest from *Bruker AXS* [54]. As presented in Sec. I, the spontaneous polarization occurs along the crystal axis b. Therefore, we deposited platinum electrodes onto the {010} faces as electrical contacts. The sample is glued between two Pt

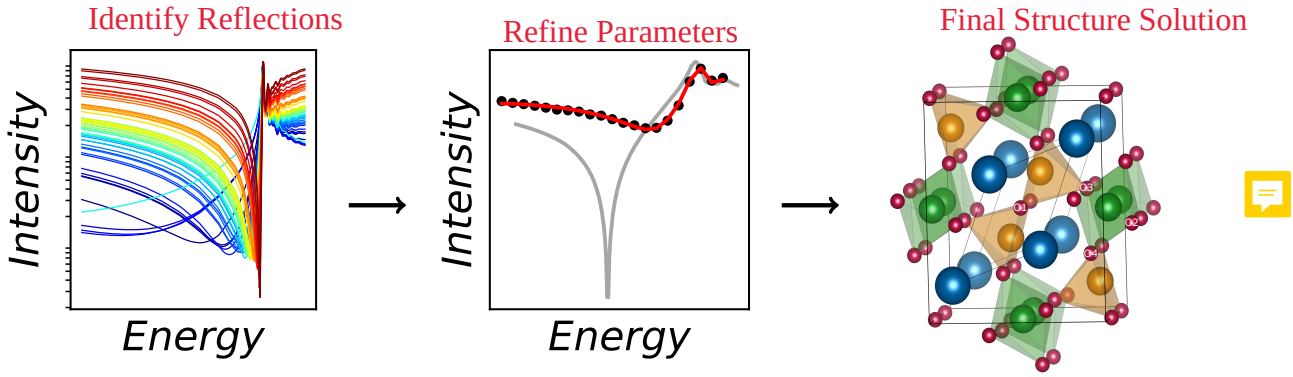

Figure 3. Left: Identification of sensitive reflections. Those reflections are characterized by a structure factor approaching zero and a respective local minimum of the energy dependent Bragg intensity, which provides contrast by several orders of magnitude. Middle: Refinement of structural parameters on the basis of the experimental data (black dots), in particular within the vicinity of the local energy minimum. By a simultanoues fit of the sensitive reflections, the relevant dynamic and static atomic displacement parameters are determined. Even minuscule displacements can be revealed (gray: tabulated structure, red: refined fit). Right: Final structure solutions with highly precise positions and ADPs (sub-pm resolution).

electrodes on a sapphire plate (setup in Fig. 5), which served as electric isolation against the cold head. This sample configuration has been used for the electric characterization as well as for biasing the forming ferroelectric domains upon cooling below T_{CM}.

B. Electric characterization of the phase transition temperature

The transition from P phase to ferroelectric CM phase induces pyroelectricity as well. Hence, in addition to the semiconducting charge transport behavior in the presence of

an external electrical field, the phase transition manifests itself in a pyroelectrical contributions to the electric current during cooling or heating. On macroscopic average, this effect can only be observed if there is a preferred orientation of domains such that the individual current contributions do not cancel each other. Therefore, we cooled the sample in a static electric field to align the domains in the CM phase [55] (more details about the experiment in SM Sec. S I) and obtain a measurable current signal, which is shown in Fig. 4.

The measurements with and without electric field show no differences in the polarization. Thus, the ferroelectric domains have a preferred orientation after phase transition to the CM phase even without external bias, as is reported in literature [24, 32, 37, 55], probably due to robust magnetic domains [24, 32, 56]. Ferroelectric switching of the polarization by a sign change of the electric field, which correspond to the findings of [32, 37, 57], was not detected. The absence of ferroelectric switching is not an intrinsic structural property and may be related to structural inhomogenities and defects, which could be removed by annealing the sample [37]. Furthermore, the pyroelectrically measured polarization depends on the history of the domain population, as previous cooling and poling processes show [24, 32]. The measured polarization without electric field is $P_s = (0.88 \pm 0.06)\,\mathrm{mC\,m^{-2}}$.

The data in Fig. 4 clearly shows the P to CM phase transition approximately at the expected temperature. To ensure stable single-phase synchrotron diffraction measurements, we therefore chose temperatures of 50 K for investigation of the P phase as well as ≈30 K and below for the CM phase.

C. Synchrotron experiment

RSD measurements were performed during two synchrotron experiments carried out at beamline BM28 (XMaS) of the *European Synchrotron Radiation Facility* (ESRF) and

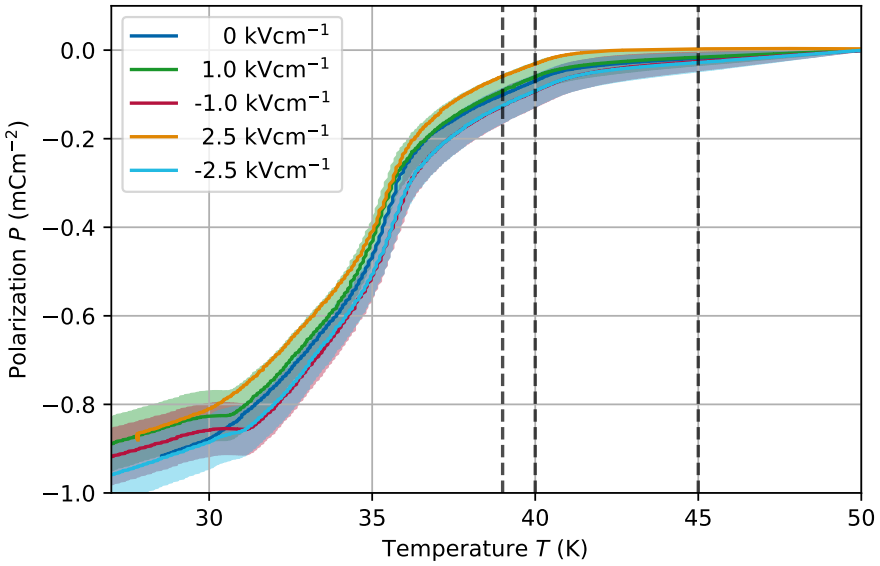

Figure 4. Temperature-dependent polarization at different electric fields (calibrated to zero at 50 K). The theoretical phase transition temperatures $T_{\mathrm{N1}} = 45\,\mathrm{K}$, $T_{\mathrm{D}} = 40\,\mathrm{K}$ and $T_{\mathrm{CM}} = 39\,\mathrm{K}$ are marked with dashed lines. A distinct jump of polarization starting below T_{CM} is clearly visible, with but equivalently pronounced also without electric field as well as with opposite poling, even above the coercive field strength of $2.2\,\mathrm{kV\,cm^{-1}}$. The lightly colored areas, indicated the error level, which mainly occurs from accuracy of the used electrometer. The determined polarizations correspond within the error range.

beamline P23 of the *Deutsches Elektronen-Synchrotron* (DESY). For each of these, a different sample holder was designed (see Fig. 5). At BM28, we glued the sample with the electrode side directly onto a platinum patch (bottom contact) of a sapphire plate, which served as electric insulation to the cooling finger. The opposite contact was realized by a thin Au wire glued to a second Pt patch on the sapphire plate (Fig. 5 (a)). For the experiment at DESY/P23 we used the same sample setup as explained in Sec. III A (see

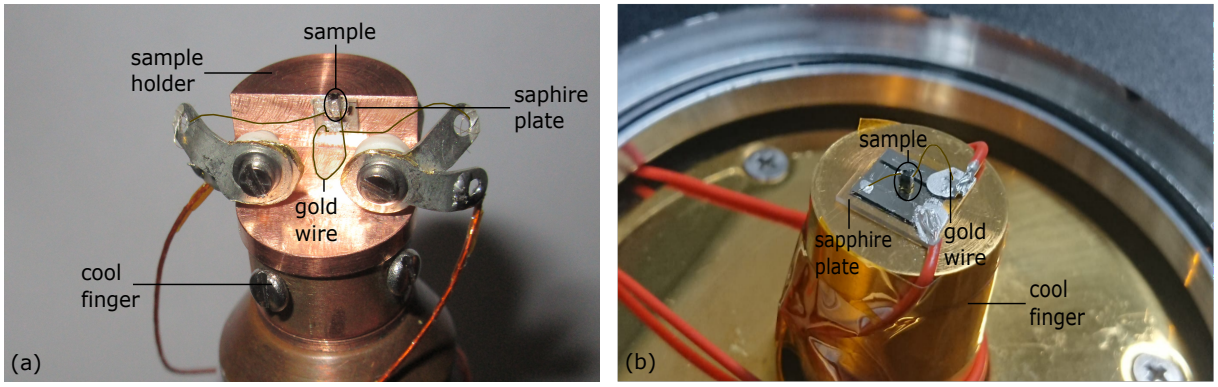

Figure 5. Electrical setup used for the experiment (a) at beamline BM28 (ESRF) with a closed cycle cryostat and (b) at beamline P23 (DESY) with a He flow cryostat.

Fig. 5 (b)).

Beamline BM28 was equipped with a 6 circle Huber diffractometer and a Pilatus3 300K 2D detector. The sample was fixed on a displex cryostat (closed cycle) with two Be domes used as X-ray vacuum window and heat shield. At beamline P23, a 5 circle diffractometer, a LAMBDA 2D detector and a He flow cryostat have been used. We measured energy dependencies (RSD spectra) of several Bragg reflections close to the Yttrium absorption edge at 17.038 keV. The sample temperature has been set above the phase transition to 50 K and below to 30 K or 25 K at ESRF/BM28 or DESY/P23, respectively. As has been confirmed from the electrical characterization, the phase transition is completed for 30 K and 25 K and only the CM phase is present (see Fig. 4). We applied an electric field of 1.0 kV cm^{-1} during the measurements below T_{CM} to align the ferroelectric domains and thus to facilitate structure analysis, although the presence of an electric field is not strictly required (*cf.* Sec. III B).

Due to the large unit cell of YMn_2O_5 and the high photon energy, the Renninger effect [58] of multiple diffraction was a major issue contaminating the data. We performed an azimuthal scan (rotation about the normal of the diffracting lattice plane) at each

reflection and each energy to eliminate contributions of the Renninger effect from the measured energy dependence [59] (more details SM Sec. S V).

In total we measured 18 reflections and obtained the respective RSD spectra to refine the P phase. Subsequently, we used the same selection of reflections to reveal the additional static displacements during the P to CM phase transition. As a result, further RSD data of these reflections below the phase transition temperature have been collected following the same procedure (azimuth-energy mesh scans). However, it is clear that static displacements along the b directions manifest themselves particularly in reflections with a large momentum transfer component along this direction.

IV. RESULTS

A. Refinement of the static and dynamic displacement parameters of the P phase

In the following section, we determine the static and dynamic displacements of the structurally well-known P phase in order to get a precise reference for the refinement of the CM phase. From the comparison of experimental and calculated RSD spectra in Fig. 6 follows that structure solutions found in crystallographic databases are not adequate to reproduce the experimental data. The observed deviations in the curves originate mainly from inaccurate ADPs, because the static structure of the P phase is well known.

The structure refinement with the RSD method is based on the multidimensional simultaneous fit of the energy dependent intensity of Bragg reflections (*cf.* SM Sec. S III). The spectra of the reflections were computed with the python package *pyasf* [60] based on the kinematic theory of diffraction, which we found suitable comparing the witdth of the rocking curve with dynamic diffraction theory (see SM Sec. S IV). Evidently, the sample is an imperfect, mosaic crystal. In addition, the studied reflections are typically weak so that extinction and other dynamic effects can be neglected. In the refinement,

we minimized relative differences of measurement and calculation, which is justified since the errors are dominated by the instrumental stability. A detailed description of all fit parameters is given in SM Sec. S III. To obtain a good agreement between modeled and measured data, we tested different approaches including ADPs in isotropic and anisotropic setting as well as the consideration of small static displacements of atoms compared to previously reported crystal structures. In the latter case, we have defined fit parameters for all atomic coordinates that are not restricted by their site symmetry. Figure 6 gives on overview about the process of the data analysis, showing the initial structure, the best fit with isotropic dynamic, anisotropic dynamic as well as anisotropic dynamic and static displacements. Details about the improvement of the fit procedure and the best fit results of these models are described in the SM Sec. S VI.

In the following, we concentrate on the most complex model with the highest number of free parameters: anisotropic ADPs with static displacements. Here, we refined 43 structural parameters (13 static and 30 dynamic displacements). The best fit result has a reduced χ^2 of 8.5×10^{-6}. All results are physically reasonable and have low error values. A further improvement of the model is not possible, since all free structural parameters within the space group have been optimized in physically reasonable ranges. Remaining discrepancies between simulation results of the best fit and experiment are due to experimental error which is dominated by the stability of the energy scans, the crystal shape and remaining Renninger effect after correction. Furthermore, the refinement of reflections with a flat minimum is difficult for the fit routine, resulting in higher discrepancies for these reflections (*e. g.* $\bar{7}44$ and $\bar{7}24$). Table I lists the ADPs obtained in the best fit result. We visualize the deviations between the refinement and the initial atomic positions (from ICSD No. 165870 [36]) in Fig. 7 with colored and grayish balls, respectively. We can now give an improved structural model for the P phase with remarkably small errors, in terms of precision and within the made assumptions, in the order of $\lessapprox$ 0.03 pm

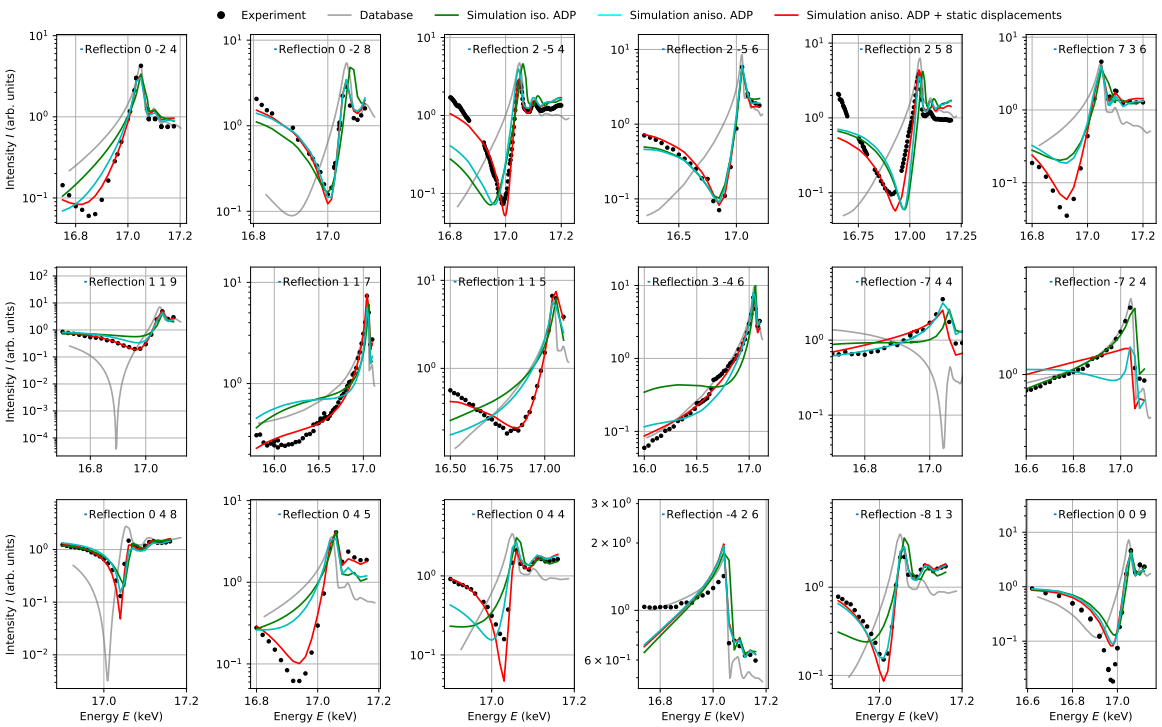

Figure 6. Experimental RSD spectra next to simulation above the phase transition temperature. The initial structure from Kagomiya *et al.* [36] (gray, $\chi^2_\nu = 1.6\times10^{-4}$), the fit results with isotropic ADPs (green, $\chi^2_\nu = 5.4\times10^{-5}$), fit results with anisotropic ADPs (cyan, $\chi^2_\nu = 3.8\times10^{-5}$) as well as the best fit results with anisotropic ADPs and static displacements (red, $\chi^2_\nu = 8.5\times10^{-6}$) are shown in comparison. Remaining discrepancies are due to systematic uncertainties and small errors from the Renninger filter routine.

for each Wyckoff position (see Tab. II).

B. Structure refinement of the CM phase

To refine the structure of the CM phase, we investigated differences in the RSD spectra above and below the phase transition (comparison of both sets of spectra, see SM Sec. S13).

Table I. Results for the anisotropic ADPs at 50 K from the best RSD fit. Errors result from the 3σ level of the reduced χ^2 distribution following [61] (see SM Sec. S VI).

	U_{11} $\left(\times 10^{-3}\,\text{Å}^2\right)$	U_{22} $\left(\times 10^{-3}\,\text{Å}^2\right)$	U_{33} $\left(\times 10^{-3}\,\text{Å}^2\right)$	U_{12} $\left(\times 10^{-3}\,\text{Å}^2\right)$	U_{13} $\left(\times 10^{-3}\,\text{Å}^2\right)$	U_{23} $\left(\times 10^{-3}\,\text{Å}^2\right)$
Y_1	0.00(156)	4.37(66)	1.53(77)	−0.99(91)		
Mn_1	0.36(111)	3.38(92)	2.44(88)	0.18(91)		
Mn_2	2.91(80)	0.00(26)	2.50(90)	−1.29(99)		
O_1	2.05(51)	0.52(67)	4.12(117)	−0.88(72)		
O_2	0.00(70)	0.31(66)	0.00(20)	−1.52(81)		
O_3	1.48(87)	0.27(60)	0.00(86)	0.35(97)		
O_4	0.01(44)	0.02(36)	1.97(77)	−1.62(71)	−1.82(68)	−1.51(82)

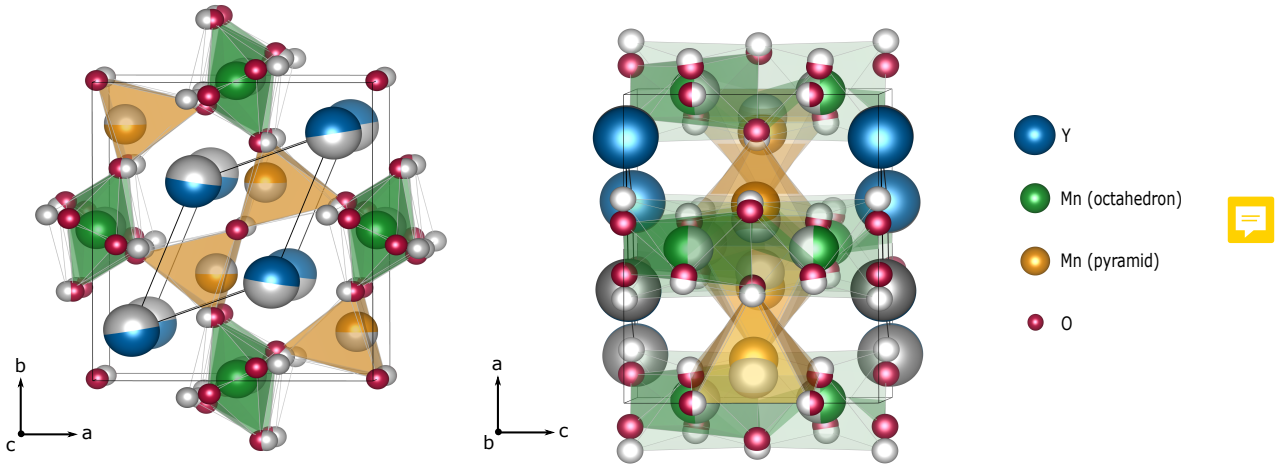

Figure 7. Visualization of the static atomic displacements before (grayish balls) based on ICSD No. 165870 [36] and after refinement of the P phase (colored balls), in two different projections. Especially the significant positional shifts within the oxygen partial structure of the P phase reflect the substantial improvement of the structure solution.

Here, we are specifically interested in changes of the local intensity minima and their location on the energy axis, which are particularly sensitive to atomic displacements [41]. These changes of the minima in the spectra are small, but significant.

Table II. Refined Wyckoff positions of YMn_2O_5 at 50 K from the results of the best fit in space group *Pbam* (55). Numbers with decimals are free parameters, whereas rational positions are fixed. Error result from the 3σ level of the reduced χ^2 distribution following [61] (see SM Sec. S VI). Additionally, we added the total displacement u for each atom ~~in pm~~.

element	label	Wyckoff symbol	x	y	z	u (pm)
Y	Y	4*g*	0.1393(4)	0.1665(2)	0	5.3(4)
Mn	Mn1	4*f*	0	1/2	0.2544(6)	1.8(5)
Mn	Mn2	4*h*	0.397(2)	0.3434(3)	1/2	12.7(13)
O	O1	4*e*	0	0	0.268(2)	1.7(9)
O	O2	4*g*	0.085(5)	0.457(2)	0	58.0(40)
O	O3	4*h*	0.125(3)	0.411(2)	0.5	25.0(30)
O	O4	8*i*	0.416(2)	0.2061(6)	0.246(3)	15.6(15)

As we know from literature and Sec. III B the spontaneous polarization emerges in crystallographic *b* direction. A lower-symmetric subgroup of the P phase space group *Pbam*, which allows polarization in *b*, is $Pb2_1m$ [62], as has been already suggested in literature [10, 17, 38]. We used the refinement results from Sec. IV A as starting model and transformed the structural parameters to the $Pb2_1m$ symmetry. In the refinement, we assumed the ADPs and machine function (see SM Sec. S III) as unchanged and only optimized the static displacement parameters, which already count a number of 50 parameters in the CM phase. Fig. 8 shows the experimental data at 25 K and 30 K, respectively, as well as the reflection intensities simulated with the refinement results of the P phase (gray) and the CM phase (red). The additional structural degrees of freedom of the CM phase significantly improve the simulated spectra ~~(red)~~ in contrast to the high-symmetry restricted spectra. The reduced χ^2 improves from 3.3×10^{-4} to 1.96×10^{-5}. The results of the refined static atomic displacements are listed in Tab. III and respective shifts are visualized compared to static displacements of the P phase in Fig. 9. Again, in terms of precision and within the made assumptions, remarkably small errors in the order of

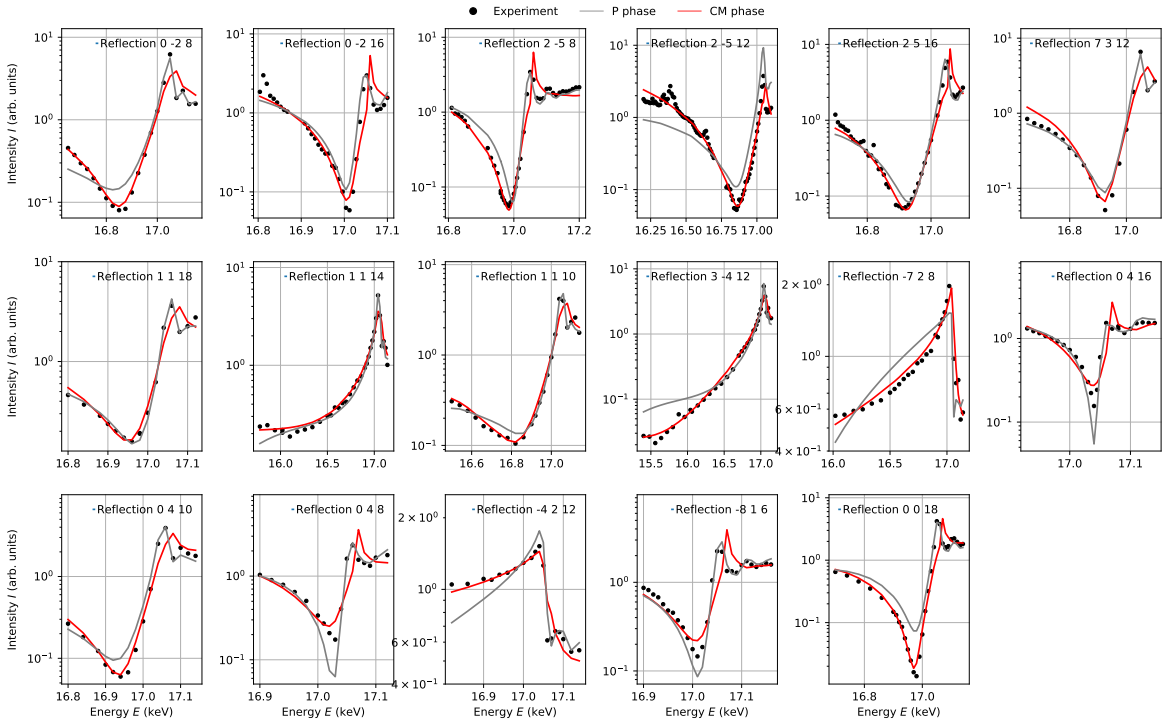

Figure 8. Simulation of RSD spectra of the refined CM phase (red) in comparison to the best refinement of the P phase (gray), as well as the experimental data below the phase transition temperature. With the additional degrees of freedom in space group $Pb2_1m$ the reduced χ^2 is improved from 3.3×10^{-4} (unrefined parameters from P phase) to 1.96×10^{-5}. The simulated RSD spectra of the CM phase show in particular an improved concordance with the most sensitive energy position of the intensity minimum.

$\lessapprox$ 0.4 pm for each coordinate on a Wyckoeff site are reached by the RSD method. The structural changes induced by the phase transition from P to CM phase incorporate total displacements u in the order of 5 pm to 58 pm.

Table III. Refined Wyckoff positions of the CM phase of YMn_2O_5 from the results of the best fit in space group $Pb2_1m(26)$. Numbers with decimals are free parameters, whereas rational positions are fixed. Errors result from the 3σ level of the reduced χ^2 distribution following [61] (see SM Sec. S VIII). Additionally, we added the shift of the y coordinate Δy and the total displacement u for each atom.

element	label	Wyck. symbol	x	y	z	Δy (pm)	u (pm)
Y	Y11	2a	0.405(4)	0.167(3)	0	0.3(30)	11(3)
Y	Y12	2a	0.109(5)	0.810(4)	0	−47(3)	20(4)
Y	Y21	2b	0.382(4)	1/6	1/2	0	5(3)
Y	Y22	2b	0.123(4)	0.848(8)	1/2	60(6)	15(6)
Mn	Mn11	4c	0.253(5)	1/2	0.121(2)	0	5(3)
Mn	Mn12	4c	0.252(5)	0.500(4)	0.632(2)	−0.1(34)	6(3)
Mn	Mn21	4c	0.670(4)	0.338(2)	0.254(3)	−13(2)	18(3)
Mn	Mn22	4c	0.847(5)	0.651(2)	0.255(4)	−16(2)	7(15)
O	O11	4c	0.27(5)	0.02(4)	0.131(7)	14(3)	18(4)
O	O12	4c	0.30(5)	−0.05(4)	0.639(7)	−42(34)	58(14)
O	O21	2a	0.39(2)	0.472(9)	0	13(8)	41(15)
O	O22	2a	0.88(3)	0.05(3)	0	8(25)	35(13)
O	O23	2b	0.39(2)	0.472(9)	1/2	13(8)	41(15)
O	O24	2b	0.88(2)	0.05(3)	1/2	8(25)	33(16)
O	O31	4c	0.38(1)	0.46(1)	0.246(4)	33(8)	42(9)
O	O32	4c	0.08(2)	0.63(2)	0.23(1)	33(16)	53(16)
O	O41	4c	0.623(2)	0.20(2)	0.135(3)	−2(16)	35(3)
O	O42	4c	0.14(1)	0.32(2)	0.137(1)	25(26)	33(13)
O	O43	4c	0.62(2)	0.24(2)	0.633(3)	33(16)	46(16)
O	O44	4c	0.14(1)	0.31(2)	0.636(1)	16(16)	28(11)

V. DISCUSSION

A. Results of the refinement of the P phase

As shown in Sec. IV A, we refined the structure of YMn_2O_5 in the P phase at 50 K with RSD and obtained small but substantial differences in atomic positions with respect

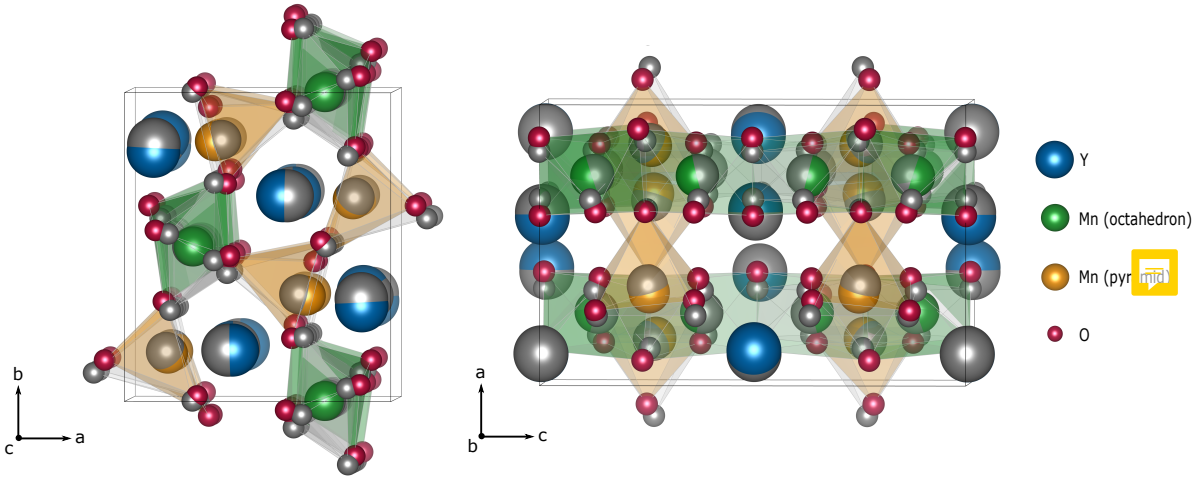

Figure 9. Visualization of the static atomic displacements (colored balls) of the CM phase in comparison to those of the P phase (gray) in two different projections. Remarkable is in particular the most prominent movement of Mn^{3+} ions outside of the pyramid's basal plane.

to the structure solution from [36], especially for the oxygen partial structure with a maximum static displacement of 58 pm, next to significantly improved values for the ADPs. The general sensitivity of the RSD method to displacements, estimated by means of the uncertainties in the structure solution of the P phase can be specified with a range between 0.4 pm to 4 pm with an average of 1.7 pm. This corresponds to the sensitivity of the RSD method, as already found in [41].

The agreement between simulation and experiment has been gradually enhanced by increasing the complexity of the underlying structure models, starting from database entries and isotropic ADPs and reaching up to anisotropic ADPs with completely uncoupled static displacements. These improvements are clearly documented in the reduction of χ^2_ν by a factor of 20, *cf.* SM Sec. S VI. In order to verify the stability of the obtained fit results and identify correlations (SM Sec. S VI), we explored the parameter space by repeating the fit with varied starting parameters while keeping selected parameters fixed

within a certain pre-defined range. To get dense projections for each fit parameter, we performed about $10^7 - 10^8$ individual fits on the TUBAF HPC cluster (ca. 350 TFlop/s CPU). Most of the parameters show no interdependencies with other parameters, only a few correlations and respective increase in the error envelopes have be found within the experimental data (see SM Sec. S VI).

B. Results of the refinement of the CM phase

Due to the high sensitivity of the RSD method to displacements in sub-pm range, we were able to refine the structure of the CM phase and can give the first structure solution of this phase in space group $Pb2_1m$ with formula per units $Z = 8$ in a $1 \times 1 \times 2$ supercell with lattice parameters $a = 7.244$ Å, $b = 8.463$ Å and $c = 11.314$ Å (Fig. 9). Again, we performed about 10^7 individual fits to get a significant statistical coverage within the parameter space for all 50 fit parameters in well-defined ranges with physical reasonable limits of ± 0.06 for all positional degrees of freedom (in fractional coordinates). To prevent a positional phase drift of the whole structure in the polar direction, we fixed one atom at the origin for all fits. Additionally, we again varied the start parameters randomly and kept two random selected parameters fixed during an individual fit to probe the development of the reduced χ^2 ~~development~~ in parameter space and to reveal parameter correlations. Most parameters converge in stable local minimum in the reduced χ^2 space, but especially parameters of a displacement in the ~~commensurately~~ doubled z direction show two minima. However, no significant linear correlations between parameters with two minima and other parameters could be found (*cf.* SM Sec. S VIII). Thus, this may be an indication for disorder in the average structure rather than for two or more classes of separate possible structure solutions. Respective correlations exhibit a pronounced fourfold symmetric-antisymmetric X-shape (Fig. S15 in SM Sec. S VIII).

Relative errors of the refined static displacement parameters are below 18 % for all

elements and for the electron-rich elements below 4 %. The refinement shows a significant movement of the ions due to the phase transition, with a maximum of 58 pm within the O partial structure, in particular within the O pyramid. Mn inside of the pyramid has a strong movement with 18 pm along the pyramidal axis, whereas Mn inside the octahedron only moves about 6 pm. Remarkably, without predefined tendency within the fit routine, the refined static displacements show an opposite movement of the positively charged Mn^{3+}/Mn^{4+} and the negatively charged O^{2-} partial structure, complying with the expected anionic/cationic movement given by the direction of the external electric field (see Δy in Tab. III). Uncertainties in the structure solution of the CM phase can be specified with a range between 3 pm to 16 pm with an average of 9.3 pm.

The refined crystallographic space group $Pb2_1m$ corresponds well with the findings from the investigation of the magnetic structure with neutron diffraction, where the magnetic point group is refined with $m2m$ [11, 32, 35] allowing a polarization in b direction, as well as with magnetoelectric measurements, which already proposed $Pb2_1m$ for the CM phase. [35]

C. Origin of ferroelectricity in the CM phase

By means of the novel RSD method, we finally discovered the atomistic origin of the ferroelectricity in the CM phase. As described in Sec. V B, the movement of the ions, especially of Mn and O partial structure, obeys the development of an oriented dipolar structure. The spontaneous polarization P_S, induced by this ionic movement, can be estimated with an approach outlined by Weigel *et al.* [63], based on considerations of Peng *et al.* [64]. With using the positional shifts $u_{j,l}$ between P phase and CM phase from experimental data for each atom j and Born Effective Charges (BEC) $Z^*_{j,kl}$ computed by

first-principle methods (for details *cf.* SM Sec. S IX), P_S can be calculated with:

$$P_{S,k} = \frac{e}{V_{\mathrm{UC}}} \sum_{j=1}^{N} Z^*_{j,kl} \cdot u_{j,l}. \tag{4}$$

Einstein's sum convention is applied for the index $l = x, y, z$ and e is the elementary charge, V_{UC} the unit cell volume, N the number of atoms in the unit cell. Here, we calculated an absolute spontaneous polarization of $P_s = (1.3 \pm 0.4)\,\mathrm{mC\,m^{-2}}$ in b direction form the experimental data. This value is in good agreement with the measured polarization (see Fig. 4, SM Sec. S I) and with measured polarization reported in literature of around $1.0\,\mathrm{mC\,m^{-2}}$ [35, 55]. The calculated P_s has the strongest contribution from the pyramids and smaller parts from the octahedrons. The vectorial contributions from the Mn partial structure are visualized in Fig. 10, which directly reflect the atomistic movement due to the phase transition. These findings match postulations in literature [12, 22, 35], which state that the displacement of the Mn^{3+} ions in the pyramid (total contribution $P_s \approx 0.04\,\mathrm{mC\,m^{-2}}$) more important for the manifestation of ferroelectricity than that of Mn^{4+} ions in the octahedron (total contribution $P_s \approx 0.0001\,\mathrm{mC\,m^{-2}}$). Additionally, we can confirm that Y is displaced [37], giving further contributions to the polarization, where the individual contribution partially compensate each other to a total $P_s \approx 0.01\,\mathrm{mC\,m^{-2}}$. The remaining contribution is due to the shift in O partial structure, especially the flexible movement of the oxygen position of the pyramid top, corner-sharing with the octahedron.

As has been summarized, the literature controversially discusses several mechanisms for magnetically driven ferroelectricty, symmetric exchange ($P_{s,\mathrm{SE}} \propto S_i \cdot S_j$, with S the spin of the magnetically active ions i and j) or antisymmetric inverse Dzyaloshinskii-Moriya interaction ($P_{s,\mathrm{DM}} \propto S_i \times S_j$) [3, 16]. For comparison, we calculated $P_{s,\mathrm{SE}} \approx 0.74\,\mathrm{mC\,m^{-2}}$ and $P_{s,\mathrm{DM}} \approx -0.08\,\mathrm{mC\,m^{-2}}$ with the magnetic moments from Kim *et al.* [27]. The findings support in particular those results that favor the contribution of both components to the polarization, but evidently the symmetric exchange interaction is predominant [12,

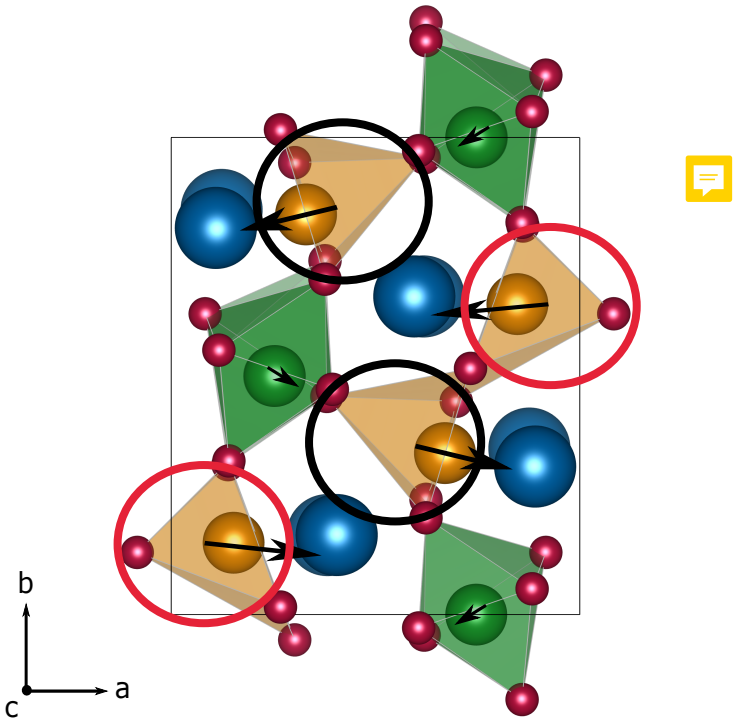

Figure 10. The resulting polarization in the CM phase of YMn_2O_5 due to structural displacements is visualized exemplary by the Mn vectorial contributions (black arrows). The main impact results in particular from the displacement of the Mn^{3+} ions with respect to the surrounding O-pyramid.

15, 16, 32]. Thus, magnetostriction due to symmetric exchange interactions shifts ions to optimize the spin-exchange energy [9, 11, 12, 22].

In addition, our results confirm that the polarization $P_s = P_{s,\mathrm{Ion}} + P_{s,\mathrm{El}}$ in the CM phase have an ionic contribution $P_{s,\mathrm{Ion}}$ induced by shifts of the ions due to the phase transition and not exclusively electronic contribution $P_{s,\mathrm{El}}$ due to spin-dependent hybridizations of O and Mn orbitals [38, 65]. Furthermore, P_s calculated from structural parameters shows a better agreement with the experimental values than an estimation of

P_s based on Spin interactions.

VI. CONCLUSION

We investigated the origin of ferroelectricity of the CM phase in YMn_2O_5 using the novel resonant X-ray diffraction method called RSD with a sensitivity to atomic displacements in pm range. We started with the refinement of dynamic and static atomic displacements of the P phase above T_{CM} to receive a highly precise structure model as a basis for structural changes during the phase transition to the CM phase. We significantly improved the structure solutions of the P phase found in crystallographic databases. For the refinement of the P phase we had in total 43 structural degrees of freedom, which converged to a stable minimum. We used the refined P phase as initial model for the refinement of the CM phase and optimized 50 static displacement parameters in space group $Pb2_1m$. With the superior confidence levels in the lowered symmetry, we present the first structural model of the CM phase in YMn_2O_5.

We successfully applied the RSD method for the first time to a significantly more complex material systems with lower symmetry and more atoms in the asymmetric unit than for our first application on $SrTiO_3$, receiving a stable and physically reasonable solution.

Next to providing new insights to the structural subtleties of the P as well as of the CM phase of YMn_2O_5, we have shown that the new RSD method is capable of refining structures with more than 50 structural degrees of freedom (for the CM phase, 30 ADPs and 13 static displacements for the P phase), based on RSD spectra of 18 reflections (compared to 4 free structural parameters in our first application of the method for polar $SrTiO_3$). The methodical advancements in this work ~~result~~ is significantly increased number of structural degrees of freedom for the YMn_2O_5 structure solutions and an improved iterative algorithm for the identification of relevant reflections (see SM Sec. S II

and Sec. S VI).

The investigations of the RSD spectra below T_{CM} show significant displacement of the ions, especially a shift of O and Mn partial structure in opposite directions. Here, the displacement of Mn^{3+} within the pyramid has the strongest contributions to the ferroelectricity. The presented findings give an answer to the origin of ferroelectrictiy in YMn_2O_5 as well as confirm structural predictions and suggestions from literature. The physical mechanism behind the ferroelectriy is magnetostriction, which shifts ions to optimize the exchange-interactions. These shifts are very small, but with the high spatial resolution of RSD, we were finally able to experimentally determine the atomistic displacements and confirm an ionic contribution to the spontaneous electric polarization.

ACKNOWLEDGMENTS

Financial support is cordially acknowledged during the projects of Deutsche Forschungsgemeinschaft (DFG; REXSuppress 324641898 and AcoustREXS 409743569) and from EU research and innovation program Horizon 2020 (CREMLINplus 871072). We acknowledge DESY (Hamburg, Germany), a member of the Helmholtz Association HGF and ESRF (Grenoble, France) for the provision of experimental facilities and beam time. The research was carried out at PETRA III/P23 (proposal I-20190565) and ESRF/BM28 (proposal MA 3817) and we would like to thank for assistance in using the beamline. Furthermore, we acknowledge the Compute Cluster 2019 of the Faculty of Mathematics and Computer Science of Technische Universität Bergakademie Freiberg, operated by the computing center (URZ) and funded by the Deutsche Forschungsgemeinschaft (DFG,

grant number 397252409) for provision of high performance computing.

[1] F. Wunderlich, T. Leisegang, T. Weißbach, M. Zschornak, H. Stöcker, J. Dshemuchadse, A. Lubk, T. Führlich, E. Welter, D. Souptel, S. Gemming, G. Seifert, and D. C. Meyer, EXAFS, XANES, and DFT study of the mixed-valence compound YMn_2O_5: Site-selective substitution of Fe for Mn, Physical Review B **82**, 014409 (2010).

[2] I. Kagomiya, H. Kimura, Y. Noda, and K. Kohn, Incommensurate antiferromagnetic ordering of ferroelectric YMn_2O_5, Journal of the Physical Society of Japan **70**, 145 (2001).

[3] H. Kimura, S. Kobayashi, S. Wakimoto, Y. Noda, and K. Kohn, Magnetically induced ferroelectricity in multiferroic compounds of $R Mn_2O_5$, Ferroelectrics **354**, 77 (2007).

[4] T. Weißbach, *Untersuchungen zu Kristallstruktur und Magnetismus von Übergangsmetalloxiden mittels Dichtefunktionaltheorie und kristallographischer experimenteller Techniken*, Dissertation, Technische Universität Bergakademie Freiberg (2010).

[5] S. Kobayashi, T. Osawa, H. Kimura, Y. Noda, I. Kagomiya, and K. Kohn, Reinvestigation of simultaneous magnetic and ferroelectric phase transitions in YMn_2O_5, Journal of the Physical Society of Japan **73**, 1593 (2004).

[6] Y. F. Popov, A. M. Kadomtseva, S. S. Krotov, G. P. Vorob'ev, and M. M. Lukina, Magnetoelectric effect in YMn_2O_5 in strong pulsed magnetic fields, Ferroelectrics **279**, 147 (2002).

[7] A. P. Pyatakov, A. M. Kadomtseva, G. P. Vorob'ev, Y. F. Popov, S. S. Krotov, A. K. Zvezdin, and M. M. Lukina, Nature of unusual spontaneous and field-induced phase transitions in multiferroics $R Mn_2O_5$, Journal of Magnetism and Magnetic Materials **321**, 858 (2009).

[8] M. Tachibana, K. Akiyama, H. Kawaji, and T. Atake, Lattice effects in multiferroic $R Mn_2O_5$ (R = Sm–Dy, Y), Physical Review B **72**, 224425 (2005).

[9] L. C. Chapon, P. G. Radaelli, G. R. Blake, S. Park, and S.-W. Cheong, Ferroelectricity

induced by acentric spin-density waves in YMn_2O_5, Physical Review Letters **96**, 097601 (2006).

[10] G. Giovanetti and J. v. d. Brink, Electronic correlations decimate the ferroelectric polarization of multiferroic $HoMn_2O_5$, Physical Review Letters **100**, 227603 (2008).

[11] L. C. Chapon, G. R. Blake, M. J. Gutmann, S. Park, N. Hur, P. G. Radaelli, and S.-W. Cheong, Structural Anomalies and Multiferroic Behavior in Magnetically Frustrated $TbMn_2O_5$, Physical Review Letters **93**, 177402 (2004).

[12] C. Vecchini, L. C. Chapon, P. J. Brown, T. Chatterji, S. Park, S.-W. Cheong, and P. G. Radaelli, Commensurate magnetic structures of $R\mathrm{Mn}_2\mathrm{O}_5$ (R = Y, Ho, Bi) determined by single-crystal neutron diffraction, Physical Review B **77**, 134434 (2008).

[13] H. Kimura, S. Kobayashi, Y. Fukuda, T. Osawa, Y. Kamada, Y. Noda, I. Kagomiya, and K. Kohn, Spiral spin structure in the commensurate magnetic phase of multiferroic $R\mathrm{Mn}_2\mathrm{O}_5$, Journal of the Physical Society of Japan **76**, 074706 (2007).

[14] A. B. Sushkov, R. Valdés Aguilar, S. Park, S.-W. Cheong, and H. D. Drew, Electromagnons in multiferroic YMn_2O_5 and $TbMn_2O_5$, Physical Review Letters **98**, 027202 (2007).

[15] R. Masuda, Y. Kaneko, Y. Yamasaki, Y. Tokura, and Y. Takahashi, Role of commensurability of spin order for optical magnetoelectric effect with electromagnons in multiferroic YMn_2O_5, Physical Review B **96**, 041117 (2017).

[16] S. Wakimoto, H. Kimura, Y. Sakamoto, M. Fukunaga, Y. Noda, M. Takeda, and K. Kakurai, Role of magnetic chirality in polarization flip upon a commensurate-incommensurate magnetic phase transition in YMn_2O_5, Physical Review B **88**, 140403 (2013).

[17] S. Baidya, P. Sanyal, H. Das, B. Roessli, T. Chatterji, and T. Saha-Dasgupta, Understanding neutron scattering data in YMn_2O_5: An effective spin Hamiltonian, Physical Review B **84**, 054444 (2011).

[18] Z. H. Chen, R.-J. Xiao, C. Ma, Y.-B. Qin, H.-L. Shi, Y.-J. Song, Z. Wang, H.-F. Tian, H.-X. Yang, and J.-Q. Li, Electronic structure of YMn_2O_5 studied by EELS and first-principles

calculations, Frontiers of Physics **7**, 429 (2012).

[19] Y. Noda, H. Kimura, Y. Kamada, T. Osawa, Y. Fukuda, Y. Ishikawa, S. Kobayashi, Y. Wakabayashi, H. Sawa, N. Ikeda, and K. Kohn, Relation between ferroelectric and antiferromagnetic order in $R\mathrm{Mn_2O_5}$, Physica B: Condensed Matter **385-386**, 119 (2006).

[20] Y. Noda, H. Kimura, Y. Kamada, and Ishikawa, Lattice modulation in $\mathrm{YMn_2O_5}$ and $\mathrm{TbMn_2O_5}$ studied by using synchrotron radiation X-ray, Journal of the Korean Physical Society **51**, 828 (2007).

[21] Y. Noda, H. Kimura, M. Fukunaga, S. Kobayashi, I. Kagomiya, and K. Kohn, Magnetic and ferroelectric properties of multiferroic $R\mathrm{Mn_2O_5}$, Journal of Physics: Condensed Matter **20**, 434206 (2008).

[22] S.-W. Cheong and M. Mostovoy, Multiferroics: a magnetic twist for ferroelectricity, Nature Materials **6**, 13 (2007).

[23] M. Deutsch, T. C. Hansen, M. T. Fernández-Díaz, A. Forget, D. Colson, F. Porcher, and I. Mirebeau, Pressure-induced commensurate phase with potential giant polarization in $\mathrm{YMn_2O_5}$, Physical Review B **92**, 060410(R) (2015).

[24] M. Fukunaga and Y. Noda, Classification and interpretation of the polarization of multiferroic $R\mathrm{Mn_2O_5}$, Journal of the Physical Society of Japan **79**, 054705 (2010).

[25] T.-C. Han and J. G. Lin, R-dependent magnetic and structural properties in $R\mathrm{Mn_2O_5}$ with R = Y, Er, Ho, Dy, and Tb, Journal of Applied Physics **99**, 08J508 (2006).

[26] A. M. Kadomtseva, S. S. Krotov, Y. F. Popov, and G. P. Vorob'ev, Features of the magnetoelectric behavior of the family of multiferroics $R\mathrm{Mn_2O_5}$ at high magnetic fields (Review), Low Temperature Physics **32**, 709 (2006).

[27] J.-H. Kim, S.-H. Lee, S. Park, M. Kenzelmann, A. B. Harris, J. Schefer, J.-H. Chung, C. Majkrzak, M. Takeda, S. Wakimoto, S.-W. Cheong, M. Matsuda, H. Kimura, Y. Noda, and K. Kakurai, Spiral spin structures and origin of the magnetoelectric coupling in $\mathrm{YMn_2O_5}$, Physical Review B **78**, 245115 (2008).

[28] H. Kimura, Y. Noda, and K. Kohn, Spin-driven ferroelectricity in the multiferroic compounds of $R\mathrm{Mn_2O_5}$, Journal of Magnetism and Magnetic Materials **321**, 854 (2009).

[29] K. Mukherjee, K. S. Kumar, and A. Banerjee, Observation of different spin behavior with temperature variation and Cr substitution in a multiferroic compound $\mathrm{YMn_2O_5}$, Solid State Communications **153**, 66 (2013).

[30] Y. Noda, Y. Fukuda, H. Kimura, I. Kagomiya, S. Matsumoto, K. Kohn, T. Shoubu, and N. Ikeda, Review and prospect of ferroelectricity and magnetism in $\mathrm{YMn_2O_5}$, Journal of the Korean Physical Society **42**, 1192 (2003).

[31] Y. F. Popov, A. M. Kadomtseva, S. S. Krotov, G. P. Vorob'ev, K. I. Kamilov, M. M. Lukina, and M. M. Tehranchi, Magnetic and structural phase transitions in $\mathrm{YMn_2O_5}$ ferromagnetoelectric crystals induced by a strong magnetic field, Journal of Experimental and Theoretical Physics **96**, 961 (2003).

[32] P. G. Radaelli, L. C. Chapon, A. Daoud-Aladine, C. Vecchini, P. J. Brown, T. Chatterji, S. Park, and S.-W. Cheong, Electric field switching of antiferromagnetic domains in $\mathrm{YMn_2O_5}$: A probe of the multiferroic mechanism, Physical Review Letters **101**, 067205 (2008).

[33] P. G. Radaelli, C. Vecchini, L. C. Chapon, P. J. Brown, S. Park, and S.-W. Cheong, Incommensurate magnetic structure of $\mathrm{YMn_2O_5}$, Physical Review B **79**, 020404 (2009).

[34] R. A. de Souza, U. Staub, V. Scagnoli, M. Garganourakis, Y. Bodenthin, S.-W. Huang, M. García-Fernández, S. Ji, S.-H. Lee, S. Park, and S.-W. Cheong, Magnetic structure and electric field effects in multiferroic $\mathrm{YMn_2O_5}$, Physical Review B **84**, 104416 (2011).

[35] I. Kagomiya, S. Matsumoto, K. Kohn, Y. Fukuda, T. Shoubu, H. Kimura, Y. Noda, and N. Ikeda, Lattice distortion at ferroelectric transition of $\mathrm{YMn_2O_5}$, Ferroelectrics **286**, 167 (2003).

[36] I. Kagomiya, K.-I. Kakimoto, and H. Ohsato, Precursor phenomenon on ferroelectric transition in multiferroic $\mathrm{YMn_2O_5}$, Journal of the European Ceramic Society **30**, 255 (2010).

[37] A. Inomata and K. Kohn, Pyroelectric effect and possible ferroelectric transition of helimagnetic $GdMn_2O_5$, $TbMn_2O_5$ and YMn_2O_5, Journal of Physics: Condensed Matter **8**, 2673 (1996).

[38] S. Partzsch, S. B. Wilkins, J. P. Hill, E. Schierle, E. Weschke, D. Souptel, B. Büchner, and J. Geck, Observation of electronic ferroelectric polarization in multiferroic YMn_2O_5, Physical Review Letters **107**, 057201 (2011).

[39] J. P. Attfield, Resonant powder x-ray diffraction, in *Materials Science Forum*, Vol. 228 (Trans. Tech. Publ., 1996) p. 201.

[40] U. Vainio, K. Pirkkalainen, K. Kisko, G. Goerigk, N. E. Kotelnikova, and R. Serimaa, Copper and copper oxide nanoparticles in a cellulose support studied using anomalous small-angle X-ray scattering, The European Physical Journal D **42**, 93 (2007).

[41] C. Richter, M. Zschornak, D. V. Novikov, E. Mehner, M. Nentwich, J. Hanzig, S. Gorfman, and D. C. Meyer, Picometer polar atomic displacements in strontium titanate determined by resonant X-ray diffraction, Nature Communications **9**, 178 (2018).

[42] C. Richter, D. V. Novikov, E. K. Mukhamedzhanov, M. M. Borisov, K. A. Akimova, E. N. Ovchinnikova, A. P. Oreshko, J. Strempfer, M. Zschornak, E. Mehner, D. C. Meyer, and V. E. Dmitrienko, Mechanisms of the paraelectric to ferroelectric phase transition in RbH_2PO_4 probed by purely resonant X-ray diffraction, Physical Review B **89**, 094110 (2014).

[43] M. Zschornak, C. Richter, M. Nentwich, H. Stöcker, S. Gemming, and D. C. Meyer, Probing a crystal's short-range structure and local orbitals by Resonant X-ray Diffraction methods, Crystal Research and Technology **49**, 43 (2014).

[44] M. Zimmermann, C. S. Nelson, J. P. Hill, D. Gibbs, M. Blume, D. Casa, B. Keimer, Y. Murakami, C.-C. Kao, C. Venkataraman, T. Gog, Y. Tomioka, and Y. Tokura, X-ray resonant scattering studies of orbital and charge ordering in $Pr_{1-x}Ca_xMnO_3$, Physical Review B **64**, 195133 (2001).

[45] Y. Murakami, H. Kawada, H. Kawata, M. Tanaka, T. Arima, Y. Moritomo, and Y. Tokura, Direct observation of charge and orbital ordering in $La_{0.5}Sr_{1.5}MnO_4$, Physical Review Letters **80**, 1932 (1998).

[46] V. E. Dmitrienko and E. N. Ovchinnikova, Resonant X-ray diffraction: 'forbidden' Bragg reflections induced by thermal vibrations and point defects, Acta Crystallographica Section A: Foundations of Crystallography **56**, 340 (2000).

[47] B. Bohnenbuck, I. Zegkinoglou, J. Strempfer, C. S. Nelson, H.-H. Wu, C. Schüßler-Langeheine, M. Reehuis, E. Schierle, P. Leininger, T. Herrmannsdörfer, J. C. Lang, G. Srajer, C. T. Lin, and B. Keimer, Magnetic structure of $RuSr_2GdCu_2O_8$ determined by resonant X-Ray diffraction, Physical Review Letters **102**, 037205 (2009).

[48] V. Scagnoli, U. Staub, A. M. Mulders, M. Janousch, G. I. Meijer, G. Hammerl, J. M. Tonnerre, and N. Stojic, Role of magnetic and orbital ordering at the metal-insulator transition in $NdNiO_3$, Physical Review B **73**, 100409 (2006).

[49] J. Hanzig, M. Zschornak, F. Hanzig, E. Mehner, H. Stöcker, B. Abendroth, C. Röder, A. Talkenberger, G. Schreiber, D. Rafaja, S. Gemming, and D. C. Meyer, Migration-induced field-stabilized polar phase in strontium titanate single crystals at room temperature, Physical Review B **88**, 024104 (2013).

[50] M. Newville, T. Stensitzki, D. B. Allen, M. Rawlik, A. Ingargiola, and A. Nelson, LMFIT: Non-linear least-square minimization and curve-fitting for Python, Astrophysics Source Code Library, 1606 (2016).

[51] D. C. Meyer, A. Kupsch, and P. Paufler, Absorption and extinction correction in quantitative DAFS analysis, Journal of Synchrotron Radiation **10**, 144 (2003).

[52] K. N. Trueblood, H.-B. Bürgi, H. Burzlaff, J. D. Dunitz, C. M. Gramaccioli, H. H. Schulz, U. Shmueli, and S. C. Abrahams, Atomic displacement parameter nomenclature. Report of a subcommittee on atomic displacement parameter nomenclature, Acta Crystallographica Section A: Foundations of Crystallography **52**, 770 (1996).

[53] D. Souptel, Crystal growth and properties of the novel multiferroic oxide compounds (2007).

[54] Bruker AXS Inc., *DOC-M86-EXX190 D8 QUEST User Manual* (2012).

[55] R. P. Chaudhury, C. R. dela Cruz, B. Lorenz, Y. Y. Sun, C. W. Chu, S. Park, and S.-W. Cheong, Control of ferroelectric polarization in multiferroic YMn_2O_5 by external pressure, Journal of Physics: Conference Series **150**, 042013 (2009).

[56] M. Fukunaga and Y. Noda, New technique for measuring ferroelectric and antiferroelectric hysteresis loops, Journal of the Physical Society of Japan **77**, 064706 (2008).

[57] R. Chaudhury, C. R. dela Cruz, B. Lorenz, Y. Sun, C. W. Chu, S. Park, and S.-W. Cheong, Pressure-induced polarization reversal in multiferroic YMn_2O_5, Physical Review B **77**, 220104 (2008).

[58] M. Renninger, 'Umweganregung', eine bisher unbeachtete Wechselwirkungserscheinung bei Raumgitterinterferenzen, Zeitschrift für Physik **106**, 141 (1937).

[59] M. Nentwich, M. Zschornak, T. Weigel, T. Köhler, N. D., D. C. Meyer, and C. Richter, Treatment of Multiple Beam X-ray Diffraction in Energy Dependent Measurements, Journal of Synchrotron Radiation (2023), (in progress).

[60] C. Richter, pyasf – symbolic computing of anisotropic resonant scattering factor, GitHub repository, `https://github.com/carichte/pyasf` (2020).

[61] Y. Avni, Energy spectra of X-ray clusters of galaxies, The Astrophysical Journal **210**, 642 (1976).

[62] IUCr, *International Tables for Crystallography, Volume A: Space Group Symmetry*, 5th ed., edited by T. Hahn, International Tables for Crystallography (Kluwer Academic Publishers, Dordrecht, Boston, London, 2002).

[63] T. Weigel, C. Ludt, T. Leisegang, E. Mehner, S. Jachalke, H. Stöcker, D. C. Meyer, and M. Zschornak, Determining the pyroelectric coefficient of lithium niobate and lithium tantalate from structural data, Physical Review B (2023), (in progress).

[64] Q. Peng and R. E. Cohen, Origin of pyroelectricity in $LiNbO_3$, Physical Review B **83**,

220103 (2011).

[65] S. Partzsch, S. B. Wilkins, E. Schierle, J. E. Hamann-Borrero, H. Wadati, V. Soltwisch, J. P. Hill, E. Weschke, D. Souptel, B. Büchner, and J. Geck, Resonant soft X-ray scattering studies of multiferroic YMn_2O_5, The European Physical Journal: Special Topics **208**, 133 (2012).